Available online at www.sciencedirect.com
ScienceDirect
Journal of the European Ceramic Society 29 (2009) 1625–1630
www.elsevier.com/locate/jeurceramsoc

Creep mechanisms of laminated alumina/zirconia-toughened alumina composites

A. Morales-Rodríguez [a], A. Domínguez-Rodríguez [a], G. de Portu [b], M. Jiménez-Melendo [a,*]

[a] *Departamento de Física de la Materia Condensada, Universidad de Sevilla, Aptdo. 1065, 41080 Sevilla, Spain*
[b] *Institute of Science and Technology for Ceramics (ISTEC-CNR), Via Granarolo 64, Faenza, Italy*

Received 12 August 2008; received in revised form 19 September 2008; accepted 24 September 2008
Available online 5 November 2008

Abstract

High-temperature plastic deformation of laminar composites containing alternate layers of Al_2O_3 and a mixture of 60 vol.% Al_2O_3 + 40 vol.% 3 mol% Y_2O_3-stabilized tetragonal ZrO_2 (ZTA) produced by tape casting is investigated in isostrain compression testing at temperatures between 1400 and 1500 °C. The stress exponent n and the creep activation energy Q are close to 1 and 700 kJ/mol, respectively. Microstructual observations reveal the lack of differential features in the ZTA layers and a general creep damage of the Al_2O_3 layers, with little microcracking by cavity coalescence even up to strains of 30%. The layer interfaces maintain their initial structural integrity after testing. An isostrain composite creep model predicts correctly the overall mechanical behavior of the laminates, which is dictated by the alumina phase via diffusional creep controlled by oxygen grain boundary diffusion.

Keywords: Creep; Al_2O_3; ZrO_2; Composites; Laminates

1. Introduction

In the last years, new strategies based on the development of ceramic/ceramic lamellar structures have emerged in order to improve the mechanical performance of ceramics for structural applications.[1–3] These structures provide a unique opportunity for tailoring the mechanical properties and meeting apparently contradictory characteristics of structural ceramics. Al_2O_3- and ZrO_2-based ceramics have been preferentially used as starting materials to build up layered microarchitectures because of their excellent mechanical properties. For example, large improvements in strength and fracture toughness at room temperature have been achieved in alumina/zirconia laminar composites because of various crack-shielding phenomena related to the presence of the layers.[4–7] It has also been shown that the laminar microarchitecture beneficially influences the high-temperature creep properties of layered ceramics, conjugating the ductility and creep resistance of the monolithic constituents.[8,9]

The creep behavior of alumina/zirconia-toughened alumina (ZTA) laminated composites with strong interfaces has been previously evaluated in the isostress condition (stress axis perpendicular to layer planes). It was found[10] that the overall creep behavior of the laminates was controlled by the softer phase (ZTA), but with, superior creep resistance than its monolithic counterpart because of the constraints imposed by the harder phase through interface bonding. In the present study, Al_2O_3/ZTA laminated composites were fabricated by warm pressing and sintering of layers produced by tape casting. The objective of this work is to characterize the high-temperature mechanical behavior of these materials, when loaded axially in compression (stress axis parallel to layer planes) and to generate the predictive rate equation for correlating microstructural and mechanical data.

2. Experimental procedure

Sheets of pure-alumina and 60 vol.% Al_2O_3 + 40 vol.% 3 mol% Y_2O_3-stabilized tetragonal ZrO_2 (ZTA) were prepared by tape casting; details of the fabrication process can be found elsewhere.[9] Discs with a diameter of 40 mm were cut from the green ceramic sheets and then stacked and warm-pressed

* Corresponding author.
E-mail address: melendo@us.es (M. Jiménez-Melendo).

0955-2219/$ – see front matter © 2008 Elsevier Ltd. All rights reserved.
doi:10.1016/j.jeurceramsoc.2008.09.017

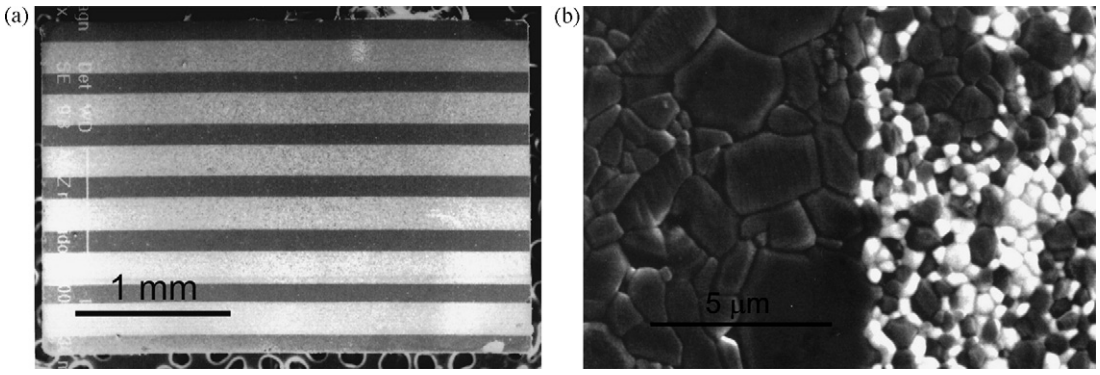

Fig. 1. SEM micrographs of Al_2O_3/ZTA multilayer composites. (a) Low magnification (dark layers are Al_2O_3, bright layers are ZTA). (b) Detail of an interface between the Al_2O_3 layer and the ZTA layer; the latter one is formed by zirconia grains (bright phase) and alumina grains (dark phase).

at 80 °C for 30 min at 30 MPa. The structure was designed to have alumina layers as outer surfaces. The laminated samples were finally sintered at 1550 °C for 1 h in air. After sintering, the density of the samples, measured by Archimedes' method, was close to the theoretical density.

For mechanical testing, rectangular specimens of about 4 mm × 2 mm × 2 mm were cut from the laminated compacts with the largest dimension (the loading axis) parallel to the layer interfaces. In such configuration, isostrain and thus isostrain-rate conditions will apply through the deformation process. Compressive tests were carried out at constant cross-head speeds between 5 and 50 μm/min (corresponding to initial strain rates strain rates $\dot{\varepsilon}_o$ between 2×10^{-5} and 2×10^{-4} s^{-1}) and at constant load (5–120 MPa) in air at temperatures between 1400 and 1500 °C. The recorded data at constant strain rate, load F versus time t, and at constant load, instantaneous specimen length $l(t)$ versus time t, were plotted, respectively, as $\sigma - \varepsilon$ and log $\dot{\varepsilon} - \varepsilon$ curves, where $\sigma = F/S_0$ (with S_0 the initial cross-sectional area of the sample) is the nominal stress, $\varepsilon = -\ln[l(t)/l_0]$ (with l_0 the initial length of the sample) is the true strain and $\dot{\varepsilon}$ the strain rate. Mechanical data were analyzed using the standard high-temperature power law for steady-state deformation:

$$\dot{\varepsilon} = A\sigma^n d^{-p} \exp\left(-\frac{Q}{RT}\right) \quad (1)$$

where A is a parameter depending on the deformation mechanism, n the stress exponent, p the grain size exponent, Q the activation energy for flow and RT has the usual meaning.

The microstructural characterization of the as-received and deformed laminates was carried out using scanning electron microscopy (Microscopy Service, University of Sevilla, Spain). To this end, perpendicular sections to the layer interfaces were cut from the samples, mechanically polished and then thermally etched at 1350 °C for 30 min in air to reveal grain boundaries. The morphological parameters of the various phases were characterized by using a semiautomatic image analyzer.

3. Experimental results

Fig. 1(a) shows a low magnification SEM micrograph of the as-received laminated composite cross-section, consisting of seven layers of alumina (dark phase) 125-μm thick and six layers of ZTA (bright phase) 215-μm thick; the corresponding volume fractions are $f_{Al} = 0.40$ and $f_{ZTA} = 0.60$. The two types of layers are well defined with very straight interfaces (Fig. 1(a) and (b)). Alumina grains in the Al_2O_3 layers have an average grain size d (taken as the spatial grain size) of 1.2 μm. The ZTA layer shows the typical equiaxed duplex microstructure of such composites (Fig. 1(b)), formed by alumina grains (dark phase) of $d = 0.6$ μm and slightly smaller zirconia grains of $d = 0.4$ μm. The smaller size of the Al_2O_3 grains in the ZTA layer, in comparison to those in the Al_2O_3 layer, is due to the presence of the second dispersed phase, which produces a fine-grained microstructure that is remarkably resistant to coarsening at elevated temperatures.[11] This enhanced microstructural stability of ZTA composites has been widely exploited to achieve superplasticity.[12–14]

Fig. 2 displays a $\sigma - \varepsilon$ curve at 1500 °C showing several strain rates changes which allow the determination of the stress exponent by using Eq. (1). Reasonable steady-state stresses were achieved at every rate change, except at the higher strain rate imposed where the specimen started to fail. At lower temperatures, the composites failed at correspondingly lower strain

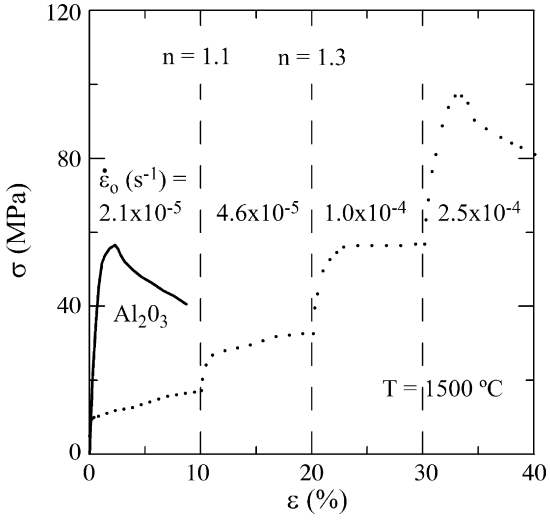

Fig. 2. Stress–strain curve at 1500 °C of laminated composite deformed under isostrain condition (points). Several determinations of the stress exponent n by strain rate changes are shown. The curve of high-purity monolithic alumina at the initial strain rate of $\dot{\varepsilon}_o = 2 \times 10^{-5}$ s^{-1} is also shown.

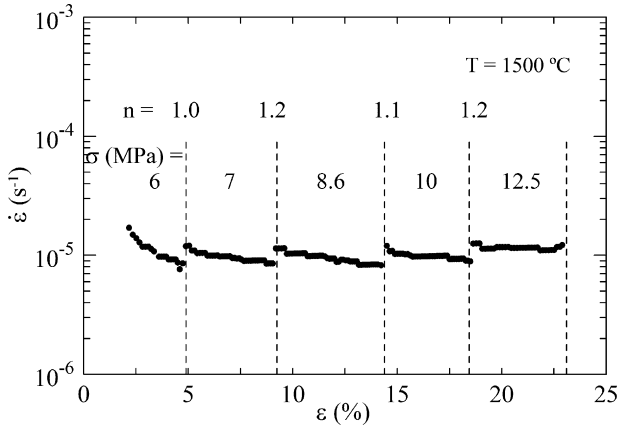

Fig. 3. Creep curve at constant load plotted as log $\dot{\varepsilon} - \varepsilon$ for laminated composite deformed under isostrain condition. Several determinations of the stress exponent n by stress changes are shown.

rates. The measured stress exponent is close to unity, indicating a Newtonian creep process. Fig. 2 also shows the $\sigma - \varepsilon$ curve at $\dot{\varepsilon}_o = 2 \times 10^{-5}\,s^{-1}$ of high-purity monolithic Al_2O_3 with an average grain size $d = 1.8\,\mu m$, similar to that of the alumina layers. The monolith failed with very little plastic deformation after attaining a maximum stress σ_{max} of 55 MPa.

Fig. 3 displays a constant load creep test conducted at 1500 °C showing several load changes for determining the stress exponent n (Eq. (1)); the corresponding stresses σ were calculated using the original cross-sectional area of the sample. Again, steady-states regimes were attained after every load change (characterized by negative slopes in compression constant load tests), except in the last section of the creep curve where a controlled degradation of the specimen can be observed. The measured stress exponent is $n = 1.1 \pm 0.1$, equal to that determined from constant strain rate tests (Fig. 2). The activation energy for flow Q, measured from temperature changes $\Delta T = \pm 50\,°C$ during testing (Fig. 4) by using Eq. (1), was $Q = 710 \pm 40$ kJ/mol, regardless of stress level and temperature.

After testing, the laminates showed barrelling due to friction effects, although the layer interfaces still retained their initial

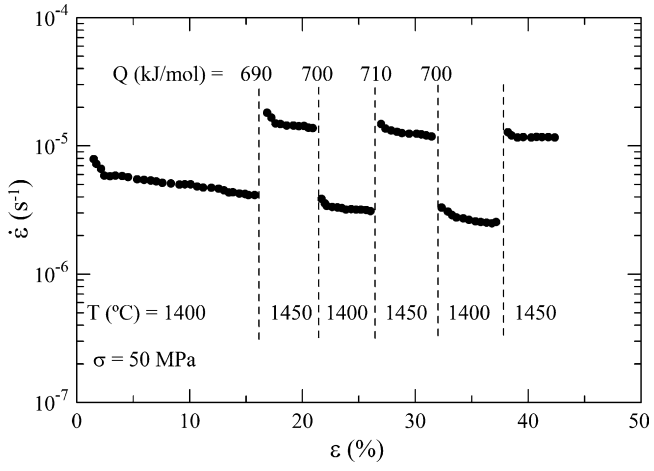

Fig. 4. Creep curve plotted as log $\dot{\varepsilon} - \varepsilon$ for a multilayer showing several determinations of the activation energy Q by temperature changes.

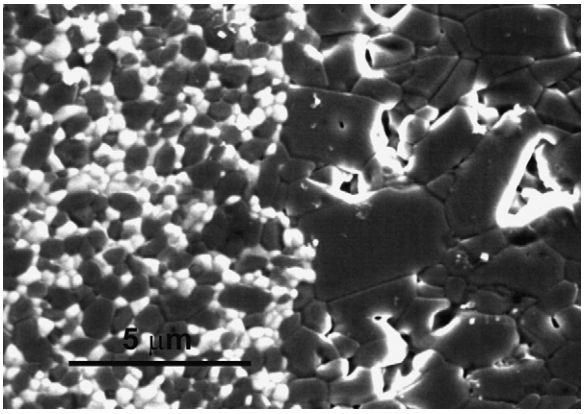

Fig. 5. SEM micrograph of a multilayer composite deformed at 1500 °C up to a final strain of 30%. Controlled cavitation occurred in the Al_2O_3 layers. The stress axis is vertical.

structural integrity, indicating an excellent interlayer adhesion (Fig. 5). No measurable change in grain size or shape during testing was observed. The ZTA layers appear almost unchanged – a consequence of its superplastic behavior, as noted above, indicating that this phase deforms preferentially by grain boundary sliding. On the other hand, the Al_2O_3 layers show extensive creep damage consisting of cavities distributed homogeneously throughout the layer, initiated at two-grain boundaries parallel to the stress direction (Fig. 5). Except for the most severe testing conditions (higher stresses or strain rates, and lower temperatures), no microcrack development by cavity coalescence was observed, thus resulting in a damage-tolerant regime. This damage mode has been reported previously in pure-alumina at low stresses, where the final failure occurs by the coalescence of creep damage at large strains.[15–17]

4. Discussion

The creep behavior of the laminates deformed in isostrain conditions is characterized by a stress exponent n and an activation energy Q of about 1 and 700 kJ/mol, respectively. In order to elucidate the creep mechanism operating in the laminates, the mechanical behavior of the composites must be compared to that of the constituent phases, alumina and ZTA, which exhibit very different creep behavior. Monolithic ZTA shows very large tensile elongations (>500%) and, correspondingly, low flow stresses. At 1500 °C, for example, the flow stress of ZTA composites[18,19] with composition and grain size similar to those in the present laminates is below 10 MPa at $\dot{\varepsilon} = 2 \times 10^{-5}\,s^{-1}$. ZTA deforms primarily by grain boundary sliding, as in superplastic metals and metallic alloys, characterized by a stress exponent $n = 2$ and an activation energy $Q = 600$–750 kJ/mol.[14] The lack of differential microstructural features of the ZTA layers in the strained laminates with respect to the as-received ones (Fig. 5) agrees with this behavior.

On the other hand, monolithic alumina is much more resistant than ZTA, with a marked brittle behavior[8,10,15] (Fig. 2). For grain sizes larger than 1 μm, it shows a stress exponent $n = 1$ and an activation energy $Q = 500$–800 kJ/mol, with very limited grain boundary sliding.[20–22] The large scatter in the reported values of

Q is probably due to the highly extrinsic character of this oxide; even a very few at.ppm of impurities/dopants change drastically the mechanical behavior.[22–25] The creep of large-grained alumina has been usually associated with a Coble diffusion creep mechanism,[20–22,26] where the transport of matter along grain boundaries is both the deformation and rate-controlling mechanism. The steady-state strain rate in the Coble model is given by the following equation:

$$\dot{\varepsilon} = \frac{150}{\pi}\frac{\sigma\Omega}{kTd^3}\delta D^{gb} \quad (2)$$

where Ω is the atomic volume, k is the Boltzmann's constant, δ is the grain boundary width and D^{gb} is the grain boundary diffusion coefficient, determined by the slower ionic specie.

The diffusion behavior in alumina is a far from simple matter today (see, for example, the recent reviews by Heuer[27] and Harding et al.[28]). Reported aluminum and oxygen diffusivities exhibit a considerable scatter, both in activation energy and in absolute magnitude of the coefficient, due probably to small variations in impurity content which significantly influence the diffusion kinetics. It must be noted, however, that oxygen diffuses slower than aluminum both in the bulk and along (sub)grain boundaries when measured on the same suite of crystals.[29,30] The creep rate of monolithic alumina (Eq. (2)) should be thus associated with oxygen diffusion along grain boundaries. Fig. 6 displays the oxygen diffusivities in bulk (D^l) and along grain boundaries (D^{gb}) measured by Prot et al.[29] in undoped and yttria-doped alumina (although contaminated with >1000 at.ppm Si), along with the corresponding activation energies. Recent data by Nakagawa et al.[31] on high-purity and yttria-doped alumina bi-crystals are also plotted in Fig. 6. Despite the scatter, the experimental data suggests that the activation energy for grain boundary diffusion is larger than for bulk diffusion.

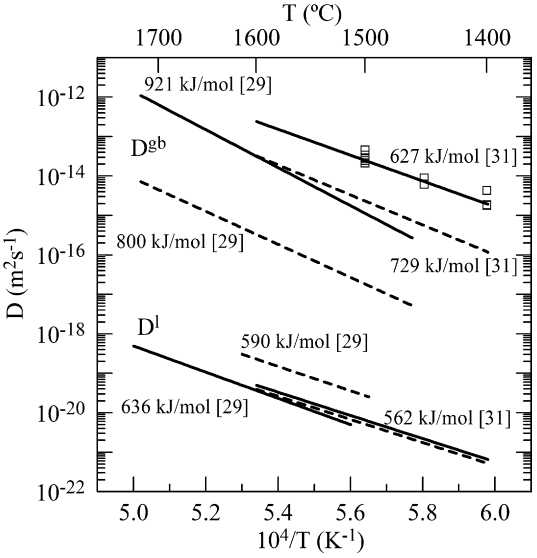

Fig. 6. Oxygen diffusivities in bulk (D^l) and along grain boundaries (D^{gb}) in undoped (solid lines) and yttrium-doped (dashed lines) alumina deduced from diffusion experiments, along with the corresponding activation energies.[29,31] Apparent diffusion coefficients deduced from creep data (Eq. (2)) are also plotted (squares).

In this study, the laminates were deformed in isostrain conditions. French et al.[32] have developed a creep model for duplex microstructures by assuming an isostress (alternate plates of each phase aligned perpendicular to the applied stress) or isostrain (plates are parallel to the applied stress) model; the latter one coincides with the configuration of the present laminates. In this case, the overall (applied) composite stress σ_c is given by the relation[32]:

$$\sigma_c = f_{Al}\sigma_{Al} + f_{ZTA}\sigma_{ZTA} \quad (3)$$

where σ_{Al} and σ_{ZTA} are the stresses supported by the Al_2O_3 and ZTA layers, respectively, and f_{Al} and f_{ZTA} the corresponding volume fractions. This model has been successfully used to explain the high-temperature mechanical behavior of laminated metal[33] and ceramic[9,34] composites. Owing to the higher creep strength of the alumina phase in comparison with ZTA, Eq. (3) can be simplified to:

$$\sigma_c = f_{Al}\sigma_{Al} \quad (4)$$

That is, the strain rate of the laminate will be controlled by the alumina phase. This is consistent with the value $n = 1$ found in the laminates, also reported in monolithic alumina.[20–22] In the isostress configuration, where the softer (ZTA) phase would be the rate-controlling phase, a stress exponent $n = 2$ was found.[10] Regarding the creep activation energy, both alumina and ZTA monoliths have Q values in the same range, which precludes a quantitative comparison.

Assuming that the alumina phase controls the overall mechanical behavior of the laminates, the diffusion coefficient D^{gb} in Eq. (2) can be deduced from the laminate creep data with $\sigma \equiv \sigma_{Al} = \sigma_c/0.40 = 2.50\sigma_c$ (Eq. (4)); δ is assumed to be 1 nm, as usual, and $\Omega = 2.20 \times 10^{-29}$ m^3. These apparent diffusion coefficients are reported in Fig. 6. The good agreement between both sets of data (diffusion and creep) confirms the validity of the previous hypothesis, i.e., the composite creep rate is primarily controlled by the Al_2O_3 layers.

Despite the apparent good agreement with pristine alumina (Fig. 6), several features suggest that the deformation of the laminates may be related to grain boundary diffusion in doped-alumina rather than in pure-alumina:

(i) EDX (energy dispersive X-ray)/SEM linescans performed across the alumina layers (Fig. 7) show the presence of yttrium and zirconium in these layers in an approximate ratio (alumina layer:ZTA layer) 1:4 and 1:9, respectively; the aluminum ratio is 2:1, in agreement with the amount of alumina in the two types of layers. Such a cation diffusion from ZTA layers towards Al_2O_3 layers is due to the elevated temperatures during sintering (1550 °C). There is no data on zirconium diffusion in alumina, but Lesage et al.[35] have reported that yttrium diffuses rapidly in polycrystalline alumina, reaching depths larger than 100 μm (the same order as the layer thickness in the laminates) after diffusion of 17 h at 1408 °C. This unintentional doping of the alumina layers explains the damage mode exhibited by the alumina layers (Figs. 5 and 7). In high-purity alumina, two

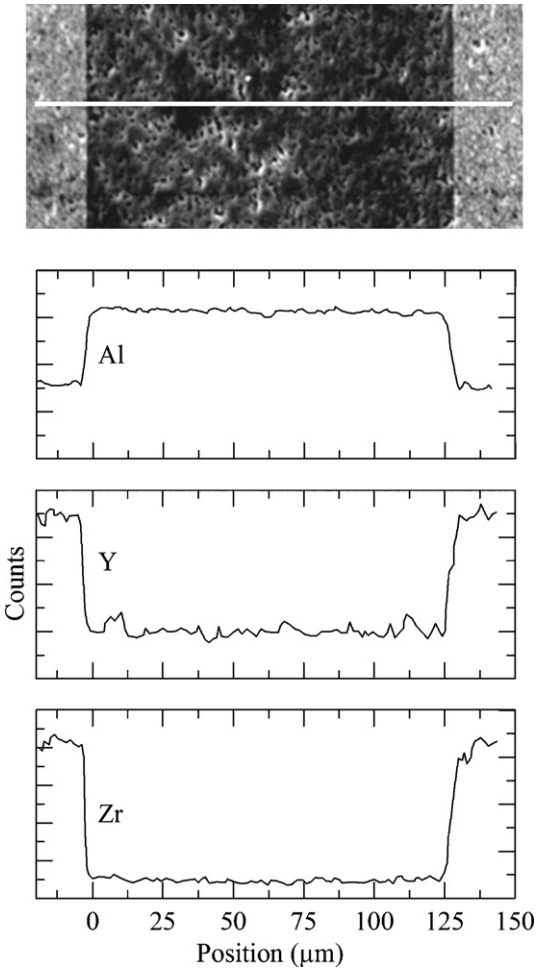

Fig. 7. EDX/SEM linescan across the alumina layer in the laminate, showing the presence of yttrium and zirconium in the layer.

failures modes have been reported.[15–17] At high stresses, the fracture is dictated by the growth of several cracks by coalescence of two-grain boundary cavities, with very small failure strains (typically <1%). At low stresses, the final failure occurs by the coalescence of creep damage, consisting of a large density of two-grain boundary cavities, at large strains (typically >20%). In the laminates, the stress carried by the alumina layers σ_{Al} is not very far from the maximum stress σ_{max} supported by high-purity monolithic alumina; for example, at 1500 °C and $\dot{\varepsilon}_o = 2 \times 10^{-5}\,s^{-1}$, $\sigma_{Al} = 2.5$, $\sigma_c \simeq 35$ MPa and $\sigma_{max} = 55$ MPa (Fig. 2), and thus a premature failure of the laminate would be expected. Because of the unintentional doping, however, such a comparison must be done with cation-doped alumina, not with pristine one. Yoshida et al.[25] have reported a decrease in creep rate higher than one order of magnitude in 0.045 mol% Y_2O_3-doped Al_2O_3 owing to segregation of yttrium at the alumina grain boundaries. A similar effect has been found with other dopant cations.[22–24] Therefore, the stress level at which the alumina layers are submitted in the laminate corresponds to a low-stress damage-tolerant regime, as experimentally observed.

(ii) The values of the apparent diffusion coefficient D^{gb} deduced from Eqs. (2) and (4) (Fig. 6) are, in fact, an upper limit of the actual values because the alumina layers support an additional in-plane stress arising from the constraint imposed by the rigid interface bonding for the strain to be the same in the soft and hard layers.[36] This additional stress, not taken into account in the simple composite creep model (Eq. (3)), should be superimposed on the applied stress (Eq. (4)), thus giving lower apparent diffusivities than those plotted in Fig. 6.

5. Conclusions

Fully dense Al_2O_3/ZTA (60 vol.% Al_2O_3 + 40 vol.% 3 mol% Y_2O_3-stabilized tetragonal ZrO_2) layered composites with uniform layers and strong interfaces have been produced starting from sheets obtained by tape casting.

Mechanical tests were performed in compression in air at constant strain rate and constant load between 1400 and 1500 °C with the loading axis parallel to the layer interfaces (isostrain configuration). After testing, the layer interfaces maintain their structural integrity. The creep parameters, stress exponent n and activation energy Q, are close to 1 and 700 kJ/mol, respectively. Except for the most severe deformation conditions, the laminates exhibit a damage-tolerant regime, characterized by an extensive grain boundary cavitation without coalescence into microcracks, reaching strains of up to 30% without failure.

An analysis based on a duplex creep model demonstrates that the alumina phase dominates the overall creep process of the laminates, accumulating more of the applied load. It is shown that diffusional creep controlled by oxygen grain boundary diffusion is consistent with mechanical data. An unintentional doping of the nominally high-purity alumina layers with yttrium and zirconium has been detected by EDX/SEM measurements, caused by the elevated temperatures of the laminate fabrication process.

Acknowledgments

The authors would like to thank the Ministerio de Ciencia y Tecnología (Spain) for the financial support through the Project No. MAT2000-1117. CNR and CSIC are also acknowledged for the financial support provided to ISTEC-CNR and Departamento de Física de la Materia Condensada (Universidad de Sevilla), in the framework of bilateral agreement.

References

1. Marshall, D. B., Design of high-toughness laminar zirconia composites. *Am. Ceram. Soc. Bull.*, 1992, **71**, 969–973.
2. Moya, J. S., Layered ceramics. *Adv. Mater.*, 1995, **7**, 185–189.
3. Harmer, M. P., Chan, H. M. and Miller, G. A., Unique opportunities for microstructural engineering with duplex and laminar ceramic composites. *J. Am. Ceram. Soc.*, 1992, **75**, 1715–1728.
4. Marshall, D. B., Ratto, J. J. and Lange, F. F., Enhanced fracture toughness in layered microcomposites of Ce–ZrO_2 and Al_2O_3. *J. Am. Ceram. Soc.*, 1991, **74**, 2979–2987.
5. Oeschner, M., Hillman, C. and Lange, F. F., Crack bifurcation in laminar ceramic composites. *J. Am. Ceram. Soc.*, 1996, **79**, 1834–1838.

6. De Portu, G., Micele, L., Guicciardi, S., Fujimura, S., Pezzotti, G. and Sekiguchi, Y., Effect of residual stresses on the fracture behaviour of notched laminated composites loaded in flexural geometry. *Compos. Sci. Technol.*, 2005, **65**, 1501–1506.
7. Lube, T., Pascual, J., Chalvet, F. and de Portu, G., Effective fracture toughness in Al_2O_3–Al_2O_3/ZrO_2 laminates. *J. Eur. Ceram. Soc.*, 2007, **27**, 1449–1453.
8. Jiménez-Melendo, M., Clauss, C., Domínguez-Rodríguez, A., Sánchez-Herencia, A. J. and Moya, J. S., Microstructure and high-temperature mechanical behavior of alumina/alumina–yttria-stabilized tetragonal zirconia multilayer composites. *J. Am. Ceram. Soc.*, 1997, **80**, 2126–2130.
9. Jiménez-Melendo, M., Clauss, C., Domínguez-Rodríguez, A., de Portu, G., Roncari, E. and Pinasco, P., High temperature plastic deformation of multilayered YTZP/ZTA composites obtained by tape casting. *Acta Mater.*, 1998, **46**, 3995–4004.
10. Jiménez-Melendo, M., Gutiérrez-Mora, F. and Domínguez-Rodríguez, A., Effect of layer interfaces on the high-temperature mechanical properties of alumina/zirconia laminate composites. *Acta Mater.*, 2000, **48**, 4715–4720.
11. Lange, F. F. and Hirlinger, M. M., Grain growth in two-phase ceramics: Al_2O_3 inclusions in ZrO_2. *J. Am. Ceram. Soc.*, 1987, **70**, 827–830.
12. Chen, I. W. and Xue, L. A., Development of superplastic structural ceramics. *J. Am. Ceram. Soc.*, 1990, **73**, 2585–2609.
13. Flacher, O., Blandin, J. J. and Plucknett, K. P., Effects of zirconia additions on the superplasticity of alumina–zirconia composites. *Mater. Sci. Eng.*, 1996, **A221**, 102–112.
14. Owen, D. M., Characteristics of superplastic deformation in dual phase alumina-zirconia composites. *Mater. Sci. Forum*, 1997, **243–245**, 405–410.
15. Robertson, A. G., Wilkinson, D. S. and Cáceres, C. H., Creep and creep fracture in hot-pressed alumina. *J. Am. Ceram. Soc.*, 1991, **74**, 915–921.
16. Wilkinson, D. S., Cáceres, C. H. and Robertson, A. G., Damage and fracture mechanisms during high-temperature creep in hot-pressed alumina. *J. Am. Ceram. Soc.*, 1991, **74**, 922–933.
17. Dalgleish, D. J., Slamovich, E. B. and Evans, A. G., Duality in the creep rupture of a polycrystalline alumina. *J. Am. Ceram. Soc.*, 1985, **68**, 575–581.
18. Kellet, B. J. and Lange, F. F., Hot forging characteristics of transformation-toughened Al_2O_3/ZrO_2 composites. *J. Mater. Res.*, 1988, **3**, 545–551.
19. Wakai, F. and Kato, H., Rheological flow in superplastic fine-grained ceramic composites. In *Ultrastructure Processing of Advanced Materials*, ed. J. D. Mackenzie and D. R. Ulrich. Wiley and Sons, New York, 1988, pp. 671–680.
20. Kottada, R. S. and Chokshi, A. H., The high temperature tensile and compressive deformation characteristics of magnesia doped alumina. *Acta Mater.*, 2000, **48**, 3905–3915.
21. Cannon, R. M., Rhodes, W. H. and Heuer, A. H., Plastic deformation of fine-grained alumina (Al_2O_3). I. Interface-controlled diffusional creep. *J. Am. Ceram. Soc.*, 1980, **63**, 46–53.
22. Yoshida, H., Yamamoto, T. and Sakuma, T., The influence of lutetium-doping effect on diffusional creep in polycrystalline Al_2O_3. *J. Eur. Ceram. Soc.*, 2003, **23**, 1795–1801.
23. Li, Y.-Z., Wang, C., Chan, H. M., Rickman, J. M., Harmer, M. P., Chabala, J. M., Gavrilov, K. L. and Levi-Setti, R., Codoping of alumina to enhance creep resistance. *J. Am. Ceram. Soc.*, 1999, **82**, 1497–1504.
24. Cho, J., Harmer, M. P., Chan, H. M., Rickman, J. M. and Thompson, A. M., Effect of yttrium and lanthanum on the tensile creep behaviour of aluminum oxide. *J. Am. Ceram. Soc.*, 1997, 1013–1017.
25. Yoshida, H., Ikuhara, Y. and Sakuma, T., High-temperature creep resistance in rare earth-doped fine-grained Al_2O_3. *J. Mater. Res.*, 1998, **13**, 2597–2601.
26. Chokshi, A. H., Diffusion creep in oxide ceramics. *J. Eur. Ceram. Soc.*, 2002, **22**, 2469–2478.
27. Heuer, A. H., Oxygen and aluminium diffusion in α-Al_2O_3: how much do we really understand? *J. Eur. Ceram. Soc.*, 2008, **28**, 1495–1507.
28. Harding, J. H., Atkinson, K. J. W. and Grimes, R. W., Experiment and theory of diffusion in alumina. *J. Am. Ceram. Soc.*, 2003, **86**, 554–559.
29. Prot, D., Le Gall, M., Lesage, B., Huntz, A. M. and Monty, C., Self-diffusion in α-Al_2O. IV. Oxigen grain-boundary self-diffusion in undoped and yttria-doped alumina polycrystals. *Phil. Mag. A*, 1996, **73**, 935–949.
30. Fielitz, P., Borchardt, G., Ganschow, S., Bertram, R. and Markwitz, A., ^{26}Al tracer diffusion in titanium doped single crystalline α-Al_2O_3. *Solid State Ionics*, 2008, **179**, 373–379.
31. Nakagawa, T., Sakaguchi, I., Shibata, N., Matsunaga, K., Mizoguchi, T., Yamamoto, T., Haneda, H. and Ikuhara, Y., Yttrium doping effect on oxygen grain boundary difusión in α-Al_2O_3. *Acta Mater.*, 2007, **55**, 6627–6633.
32. French, J. D., Zhao, J., Harmer, M. P., Chan, H. M. and Miller, G. A., Creep of duplex microstructures. *J. Am. Ceram. Soc.*, 1994, **77**, 2857–2865.
33. Grishaber, R. B., Sergueeva, A. V., Mishra, R. S. and Mukherjee, A. K., Laminated metal composites—high temperature deformation behavior. *Mater. Sci. Eng. A*, 2005, **403**, 17–24.
34. Wang, J., Taleff, E. M. and Kovar, D., High-temperature deformation of Al_2O_3/Y-TZP particulate laminates. *Acta Mater.*, 2004, **52**, 4685–4693.
35. Lesage, B., Le Gall, M., Loudjani, M. and Huntz, A. M., Yttrium diffusion in α alumina. *Defect. Diffus. Forum*, 1993, **95–98**, 1061–1064.
36. Wang, J., Taleff, E. M. and Kovar, D., Superplastic deformation of Al_2O_3/Y-TZP particulate composites and laminates. *Acta Mater.*, 2004, **52**, 5485–5491.